ELSEVIER

Catalysis Today 38 (1997) 85–95

CATALYSIS TODAY

Analysis of coke laydown in FCC catalyst through structured catalyst modelling and experimentation

O.H.J. Muhammad*, E.K.T. Kam

Petroleum Technology Department, Kuwait Institute for Scientific Research, P.O. Box 24885, 13109 Safat, Kuwait

Abstract

The Fluid Catalytic Cracking Unit (FCCU) is a complex but important refinery process to catalytically crack heavy feedstock to lighter and low sulphur products. However, catalysts are subject to deactivation by coking, metal deposition and sulphur poisoning. Any improvement in either of the process or catalyst will enhance process benefits. To get more insights into the zeolite catalyst decay, theoretical and practical aspects of coking of a commercial zeolite catalyst have been investigated. Deactivation study was carried out in a laboratory scale fluidized bed reactor to disproportionate cumene as the model reaction. The material balance over the reactor system for the cumene can be precisely determined within 4%. Two theoretical catalyst pore structured models – 'corrugated parallel bundle' and 'stochastic network' have been proposed to account for the catalyst coke deposition based on the interaction of the geometries of the coke deposit and pore structures. The prediction in coke content as a function of process time from the latter model agree well with the observed deactivation behaviour in the commercial catalyst. A number of structured catalyst parameters, which are not measurable by the existing analytical means can be estimated reliably from the models. Moreover, the coke deposition in the pore structures can be visualized.

Keywords: Structured catalyst; Coking; Corrugated parallel bundle model; Stochastic network model

1. Introduction

The continuous degrading of crude oil quality and a general shift in demand to heavy distillates demands a more effective but flexible operation in all the refining processes to maintain profit and abide by the increasingly stringent environmental regulations. The Fluid Catalytic Cracking Units (FCCUs) are one of the processes which convert straight-run atmospheric gas oil, certain atmospheric residues or heavy stocks recovered from other refining operations into high octane and low sulphur gasoline, light gas oils and olefin-rich light gases over zeolite type of catalysts [1–3]. However, the catalyst performance is strongly influenced by diffusion of reactants and products in the catalyst substrate so the overall performance is influenced by the interaction between the intrinsic kinetics and the transport processes such as heat, mass and momentum transfer in catalyst supports [4,5]. This is further complicated by the randomness of the pore networks and active unit cells which are very important to zeolite catalysts since they are mainly for resid processing to maximize the octane-barrel in FCCUs. The catalyst effectiveness also depends on the unit cell range and the matrix of the catalyst substrates, the feedstock characteristics and the accompanied deac-

*Corresponding author.

PII S0920-5861(97)00042-4

tivation contaminants such as vanadium, nickel, coke and sulphur. Most of these organo-fouling compounds found in petroleum feedstock exist in various sizes and shapes but they are predominantly in relatively large molecular structures. The optimization of the pore diameters, catalyst connectivity and access to close-end pores and hence, results numerous studies and some network models have been developed [6–12] to get insights in the diffusion, sorption and/or reaction, and deactivation in catalysts with random networks of pores.

In this contribution, the theoretical and practical aspects of the deactivation by coking of a commercial supported zeolite catalyst has been investigated. Deactivation studies were carried out in a laboratory scale fluidized bed reactor to disproportionate cumene as the model reaction. A mathematical scheme to interpret experimental data with special attention to examine the catalyst deactivation due to coke deposition on the catalyst support has been formulated at different catalyst to feed ratios. Two theoretical models have also been developed to account for the catalyst coke deposition based on the interaction of the geometries of the coke particles and the pore structures. The pore architecture employed the models can be represented by a 'corrugated parallel bundle' or 'stochastic network' pore structure. The models have been applied to correlate experimental results from which it is evident that the timewise deactivation is caused by one of the products. This scheme is also capable of estimating some structural parameters which cannot be determined by the existing analytical equipment.

2. Experiments

2.1. Experimental set-up

The super-D catalyst supplied by Crossfield Chemicals Ltd., UK, has an average diameter of 81 μ and consists of 15–18% ion exchanged Re sodium Y-zeolites on a support silica–alumina matrix. Heat treatment of catalyst particles at 150°C for 48 h is undertaken before cracking the high purity (99.5%) isopropyl benzene (cumene).

The catalytic cracking of cumene was carried out in a bench scale fluidized bed reactor made of quartz glass which holds 10 g of catalyst. A schematic

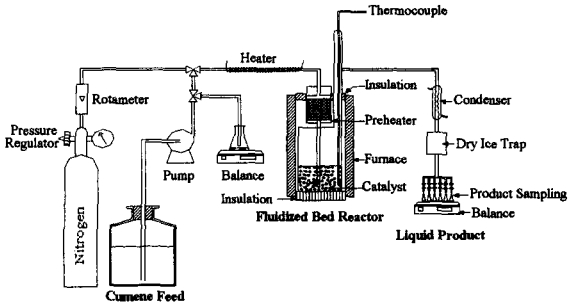

Fig. 1. Schematic of experimental apparatus for the cracking of cumene.

Table 1
Typical values of experimental parameters

Parameter	Range
Reaction temperature	475–525°C
Catalyst loading	5–10 g
Feed flowrates	0.1–5 g/min
Catalyst to feed ratio	1 : 1–100 : 1 g-cat : g-feed/min
Time on stream	1–120 min

diagram of the experimental apparatus is shown in Fig. 1 and the range of experimental parameters are given in Table 1. The reactor was purged by nitrogen gas before and after the cracking experiments. The feed flowrate was stabilized before admitting to the reactor. The feed line and the reactor were heated electrically to the required temperature which was then maintained to the nearest 1 ±° C. The reactor effluent was collected periodically and analyzed by a Pye Unicam gas liquid chromatography (GLC) containing a silicon OV17 stationary phase separation column under a temperature program. Chromatograms were quantified in terms of wt% by a Trivector Trilab 2000 integrator. The separation of all the species obtained from the product stream was excellent. The deactivated catalyst recovered after each run analyzed for coke contents using a LECO CS244 carbon/sulphur analyzer. The total surface area of the fresh and spent catalysts were measured using a Quantasorb Sortometer. The catalyst pore structures were also examined through a scanning electron microscope and images of the fresh and spent catalyst.

Before the cracking experiments, calibration was made in which several 'blank' runs at different

temperatures were carried out without catalyst to determine any conversion from thermal cracking. The maximum conversion found was about 2% which agreed well with previous works in both fixed and fluidized-bed reactor using similar type of zeolite catalysts [13]. In addition, the mass balance of cumene over the entire reaction system was undertaken to ensure no leakage as well as to form a base case for the determination of cracking conversion in the later experiments.

2.2. Fluidized bed analysis

Cumene conversion is determined from the overall mass balance over the cracking reaction system from both the normal and 'blank' runs.

$$X_d(t_i) = 1 - \frac{[P(t_i)X_c(t_i)]}{P_b(t_i)} \tag{2.1}$$

$$X_i(t) = 1 - \frac{\sum_{i=1}^{n}[P(t_i)X_c(t_i)]}{\sum_{i=1}^{n} P_b(t_i)} \tag{2.2}$$

Benzene is assumed to be the desirable product in the present development, and its selectivity, S, is defined as the moles of benzene produced per mole of cumene converted, i.e.

$$S_d(t_i) = \frac{[P(t_i)X_b(t_i)]}{[P_b(t_i)X_c(t_i)]}\left[\frac{M_c}{M_b}\right] \tag{2.3}$$

$$S_i(t) = \frac{\sum_{i=1}^{n}[P(t_i)X_b(t_i)]}{\sum_{i=1}^{n}[P_b(t_i)]}\left[\frac{M_c}{M_b}\right] \tag{2.4}$$

The normalized total benzene selectivity based on the unit mass of cumene converted per unit gram of catalyst at any time, t, can be expressed as,

$$S(t) = \frac{S_i(t)X_i(t)}{W/F} \tag{2.5}$$

where W/F is the catalyst to oil ratio.

3. Theoretical formulation

There are two theoretical developments to analyze the experimental data on cumene cracking and catalyst deactivation by coking – to perform the structured catalyst parameters estimation and to provide graphics visualization of coke deposit in pore structures.

3.1. Corrugated parallel bundle model

The model accounts for the catalyst decay by coking due to the interaction between coke geometries and pore structures. Coke is assumed to deposit randomly on the substrate macropores and in zeolite micropores resulting in both the active site coverage and pore blockage. The substrate is represented by a corrugated parallel-bundle pore structure and the zeolite is assumed to be uniformly distributed along the walls of support pores. The diffusion, reaction and deactivation occur in both the support and zeolite structures as functions of time on stream. The deactivation is in the form of coke laydown in either structure through two possible mechanisms – active site poisoning and pore plugging. Other assumptions are:

1. mass transfer is by diffusion without convection,
2. Dalton's Law of partial pressure applies,
3. total pressure is constant (i.e. molar density and total number of moles are constant),
4. first-order reaction is assumed with respect to the reactant and active surface area,
5. support and zeolite are both catalytically active, but can be deactivated differently.

Consider a single pore consisting of N elements in which the reaction is assumed to be A → Product. A mass balance for the reactant A in any pore element n, $n < N$, as shown in Fig. 2, can be expressed as:

$$\pi R_n^2 D_n \frac{d^2 C_A}{dx^2} = k_s S_n C_A \tag{3.1}$$

For the pore elements $n < N$, the boundary conditions are:

$$C_A = C_{A,n-1} \text{ at } x = 0 \tag{3.2}$$

$$C_A = C_{A,n} \text{ at } x = L$$

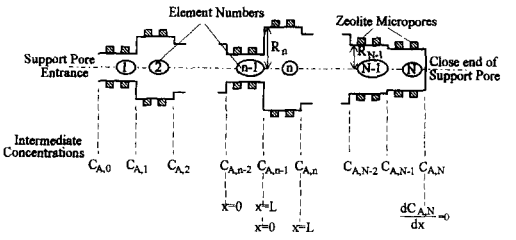

Fig. 2. A pore schematic with N elements in the corrugated parallel bundle pore model.

and the analytical solution of Eq. (3.1) becomes

$$C_A(x) = \frac{C_{A,n-1}\sinh[m_n(L-x)] - C_{A,n}\sinh(m_n x)}{\sinh(m_n L)} \tag{3.3}$$

For the close-end pore element, $n = N$, the boundary conditions are as follows:

$$C_A = C_{A,N-1} \text{ at } x = 0 \tag{3.4}$$

$$\frac{dC_A}{dx} = 0 \text{ at } x = L$$

and Eq. (3.3) becomes,

$$C_A(x) = \frac{C_{A,N-1}\cosh[m_N(L-x)]}{\cosh(m_n L)} \tag{3.5}$$

3.1.1. *Concentration profiles in the intermediate and end pore elements*

To simulate the concentration profile in the complete pore by coupling all the intermediate concentrations together, the flux between two adjacent elements must be equal, i.e.,

$$D_{n-1}R_{n-1}^2 \left.\frac{dC_A}{dx}\right|_{x=L} = D_n R_n^2 \left.\frac{dC_A}{dx}\right|_{x=0} \tag{3.6}$$

Since the catalysts are undergoing deactivation, any pore element may be either active or inactive at any specific time. Based on the pore connectivity, two common situations can be derived – two adjacent pore elements with one close-end pore, and two adjacent open-end pore elements. Due to the active conditions of the two adjacent pore elements, four different cases can exist in both the close-end pore and intermediate elements. The concentration expressions for each case can be expressed accordingly.

1. The four activity cases for two adjacent pore elements with one closed-end pore:

(a) two active elements

$$C_{A,N-2}\left[\frac{D_{N-1}R_{N-1}^2 m_{N-1}}{\sinh(m_N L)}\right] - C_{A,N-1}[D_{N-1}R_{N-1}^2 m_{N-1}\coth(m_{N-1}L) + D_N R_N^2 m_N \tanh(m_N L)] = 0 \tag{3.7a}$$

(b) one active element and one inactive element

$$C_{A,N-2} - C_{A,N-1}\cosh(m_{N-1}L) = 0 \tag{3.7b}$$

(c) one inactive element and one active element

$$C_{A,N-2}\left[\frac{D_{N-1}R_{N-1}^2}{L}\right] - C_{A,N-1}\left[\frac{D_{N-1}R_{N-1}^2}{L} + D_N R_N^2 m_n \tanh(m_N L)\right] = 0 \tag{3.7c}$$

(d) two inactive elements

$$C_{A,N-2} - C_{A,N-1} = 0 \tag{3.7d}$$

2. The four activity cases for two adjacent open-end pore elements:

(a) two active elements

$$C_{A,n-2}\left[\frac{D_{n-1}R_{n-1}^2 m_{n-1}}{\sinh(m_{n-1}L)}\right] + \left[\frac{D_n R_n^2 m_n}{\sinh(m_n L)}\right] - C_{A,n-1}[D_{n-1}R_{n-1}^2 m_{n-1}\coth(m_{n-1}L) + D_n R_n^2 m_n \coth(m_n L)] = 0 \tag{3.8a}$$

(b) one active element and one inactive element

$$C_{A,n-2}\left[\frac{D_{n-1}R_{n-1}^2 m_{n-1}}{\sinh(m_{n-1}L)}\right] + C_{A,n}\left[\frac{D_n R_n^2 m_n}{\sinh(m_n L)}\right] - C_{A,n-1}\left[D_{n-1}R_{n-1}^2 m_{n-1}\coth(m_{n-1}L) + \frac{D_n R_n^2}{L}\right] = 0 \tag{3.8b}$$

(c) one inactive element one active element

$$C_{A,n-2}\left[\frac{D_{n-1}R_{n-1}^2}{L}\right] - C_{A,n-1}\left[\frac{D_{n-1}R_{n-1}^2}{L} D_n R_n^2 m_n \coth(m_n L)\right] + C_{A,n}\left[\frac{D_n R_n^2 m_n}{\sinh(m_n L)}\right] = 0 \tag{3.8c}$$

(d) two inactive elements

$$C_{A,n-2}\left[\frac{D_{n-1}R_{n-1}^2}{L}\right] - C_{A,n-1}\left[\frac{D_{n-1}R_{n-1}^2}{L} + \frac{D_n R_n^2}{L}\right] + C_{A,n}\left[\frac{D_n R_n^2}{L}\right] = 0 \tag{3.8d}$$

3.2. *Stochastic network model*

The model consists of a network of cylindrical pores whose pore connectivity and number of dead-

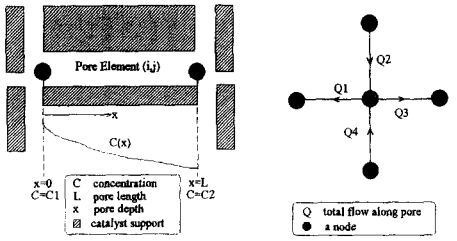

(a) Coordinates and boundary conditions in single pore element.

(b) Concentration and flow around a node of a pore network.

Fig. 3. A schematic of a pore structure in the stochastic network pore model.

end pores are randomly generated for a specified pore size distribution. For a $n \times n$ pore network, there are $2n(n+1)$ pore elements. A schematic diagram of the pore network is shown in Fig. 3 in which the boundary condition is depicted in Fig. 3(a) while the pore coordinations are given in Fig. 3(b). For a single pore element in which first-order kinetics is assumed, the mass balance can be expressed as:

$$D_n \frac{d^2 C_A}{dx^2} - k_1 C_A = 0 \tag{3.9}$$

where

$$k_1 = \frac{2k_s}{r} \tag{3.10}$$

The boundary conditions, as shown in Fig. 3(a), are:

$$C_A = C_1 \quad \text{at} \quad x = 0 \tag{3.11a}$$

and

$$C_A = C_2 \quad \text{at} \quad x = L \tag{3.11b}$$

Solve Eq. (3.9) with respect to its boundary conditions to get

$$C_A = C_1\left[\cosh\left(\frac{\phi x}{L}\right) - \sinh\left(\frac{\phi x}{L}\right)\coth\phi\right] + \frac{C_2 \sinh(\phi x/L)}{\sinh\phi}$$

where

$$\phi = L\sqrt{\frac{k_1}{D_n}} \tag{3.13}$$

And the total flow into the pore, Q, at $(x = 0)$ is given by,

$$Q = \pi r^2 \sqrt{k_1 D_n}\left[\left(\frac{C_1}{\tanh\phi}\right) - \left(\frac{C_2}{\sinh\phi}\right)\right] \tag{3.14}$$

3.2.1. Node concentration in a pore network

For a pore network, of size $n \times n$ assuming negligible reaction at the nodes, the total mass balance around a node as shown in Fig. 3(b), is:

$$\sum_{i=1}^{m} Q_i = 0 \tag{3.15}$$

When diffusion is assumed, it becomes

$$C_1 \sum_{i=1}^{m}\left[\frac{r_i^2\sqrt{D_i}}{\tanh\phi_i}\right] - \sum_{i=1}^{m}\left[\frac{C_{2i} r_i^2 \sqrt{D_i}}{\sinh\phi_i}\right] = 0 \tag{3.16}$$

In compact form, Eq. (3.16) can be written as:

$$C_1 \sum_{i=1}^{m} \alpha_i - \sum_{i=1}^{m} (C_2\beta)_i = \sum_{i=1}^{m} \gamma_i \tag{3.17}$$

where

$$\alpha_i = \frac{r_i^2\sqrt{D_i}}{\tanh\theta_i} \tag{3.18}$$

$$\beta_i = \frac{r_i^2\sqrt{D_i}}{\sinh\theta_i} \tag{3.19}$$

and

$$\gamma_i = Q_i \tag{3.20}$$

And in matrix form, it becomes:

$$AC = b \tag{3.21}$$

The solution of the above equation gives the node concentration C.

3.3. Reaction and deactivation in a pore element

The reaction and deactivation of a pore element in a corrugated parallel bundle of pores is similar to those in the stochastic pore network. The only difference occurs in the boundary conditions between the open-end pore in the corrugated parallel bundle model and the close-end pore in the stochastic network pore model. However, to estimate the reaction and deactivation rates, it is necessary to specify the

fouling mechanism and the appropriate kinetic expressions.

3.3.1. Rate of reaction in a pore element

Due to the active status of the leading (first) element in a pore, two cases can occur:

Case 1: the leading element of the pore ($n = 1$) is active

$$-r_A = -D_1 \pi R_1^2 \left[\frac{m_1 C_{A,1}}{\sinh(m_1 L)} - m_1 C_{A,0} \coth(m_1 L) \right] \tag{3.22}$$

Case 2: the leading element of the pore ($n = 1$) is inactive

$$-r_A = -D_1 \pi R_1^2 \left[\frac{C_{A,1} - C_{A,0}}{L} \right] \tag{3.23}$$

3.3.2. Active surface areas in the pores

The surface area of the pore support and zeolite can be represented by:

$$A_{OS} = \frac{R(t)}{R(0)} \tag{3.24}$$

in the pore support, and

$$S_t = \frac{S_{\mu g}}{V_g} - \sum_{i=1}^{p} \sum_{j=1}^{N} \pi R_{ij}(0) L \tag{3.25}$$

in the zeolite, respectively.

3.3.3. Rate of coking in a pore element

The coking reaction is assumed to be of first order with respect to coking precursor and support active area, then

$$-\frac{dR}{dt} = (\lambda_{cp} k_{cp} C_A + \lambda_{cs} k_{cs} C_P) A_{OS} \tag{3.26}$$

The pore coke content is composed into two parts, the coke content in the support and that in the zeolite. Consider n_c units of cubic coke of size d deposited in the support, the volume of coke $v(t)$ in a support element at any time is expressed as:

$$v(t) = n_c d^3 \tag{3.27}$$

where n_c can be obtained by:

$$n_c = \sum_{j=1}^{N} \frac{j \exp(-M) M^j}{j!} \frac{2\pi R(0) L}{d^2} \tag{3.28}$$

and

$$M = \sum_{j=1}^{N} \frac{j \exp(-M) M^j}{j!} \tag{3.29}$$

Then the total coke volume, $v_s(t)$ in all pores and elements in the parallel bundle support becomes

$$v_s(t) = 2\pi d L \sum_{i=1}^{P} \sum_{j=1}^{N} M_{ij} R_{ij}(0) \tag{3.30}$$

After normalization, the specific coke content, $V_s(t)$ in the support is

$$V_s(t) = \frac{v_s(t) V_g}{2\pi L \sum_{i=1}^{P} \sum_{j=1}^{N} R_{ij}^2(0)} \tag{3.31}$$

where V_g is the specific support pore volume.

Similarly, the coke volume in the zeolite can be obtained in terms of zeolite surface area in any pore element, A_z as

$$A_z = \exp(-M) \tag{3.32}$$

where

$$M = \frac{R(0) - R(t)}{d_z} \tag{3.33}$$

Hence the volume of coke in the zeolite is expressed as,

$$V(t) = MS(t) d_z \tag{3.34}$$

where $S(t)$ is evaluated from Eq. (3.25). The specific coke content in all the zeolite, $v_m(t)$ becomes:

$$V_m(t) = \frac{V_g d_z \sum_{i=1}^{P} \sum_{j=1}^{N} M_{ij} S_{ij}}{\sum_{i=1}^{P} \sum_{j=1}^{N} R_{ij}^2(0)} \tag{3.35}$$

Then the overall catalyst specific coke content, $V_c(t)$ is obtained by:

$$V_c(t) = V_s(t) + V_m(t) \tag{3.36}$$

The loss in zeolite volume due to coking is,

$$V_z(t) = \frac{\sum_{i=1}^{p} \sum_{j=1}^{N} V_z(t) V_g}{\sum_{i=1}^{p} \sum_{j=1}^{N} \pi R_{ij}^2(0) L} \tag{3.37}$$

4. Results and discussions

4.1. Experimental coke contents

The catalytic cracking of cumene in the fluidized bed reactor under the reaction conditions shown in Table 1, has shown that propylene, one of the products, is the main coke precursor [14]. Since the coke laydown occurs mainly on the support macropores and the zeolite micropores, the changes in catalyst structure have been monitored through surface area measurement and scanning electronic microscope image analysis [12].

The cumene conversion and benzene selectivity at the catalyst to feed ratio, $W/F = 5 : 1$ are shown in Fig. 4. The values are determined from Eqs. (2.1)–(2.5). The changes in conversion with time are plotted in a dotted line which shows an initial rapid decline in activity and then it is followed by a more graduated loss in activity. The benzene selectivity expressed as a function cumene conversion is represented by the solid line which also shows an initial steep drop in selectivity at the cumene conversion below 15%. This is followed by a period of steady selectivity when the conversion is between 15 to 45%. Another sharp drop in selectivity is observed thereafter and reaches the minimum when the conversion is at its maximum of 60%.

The results of the catalyst coke content at 3 catalyst to feed ratios, W/F : 1, 5 and 15 : 1 are shown in Fig. 5. The general trends of catalytic deactivation due to series fouling are exhibited in which a very rapid coke buildup occurs initially in catalyst pores and then levels off gradually. The coke buildup at higher W/F is more than that at lower W/F values. This is

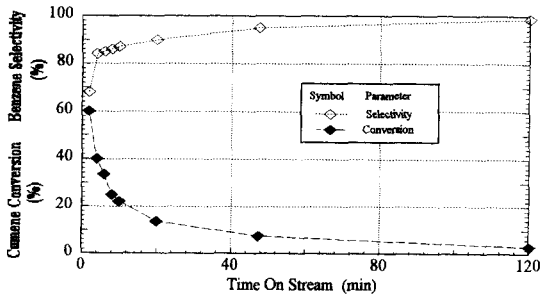

Fig. 4. Experimental result of cumene conversion and benzene selectivity at $W/F = 5$.

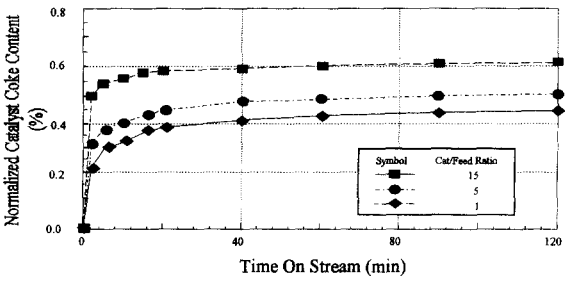

Fig. 5. Experimental results of catalyst/feed ratio effect on catalyst coke content with time.

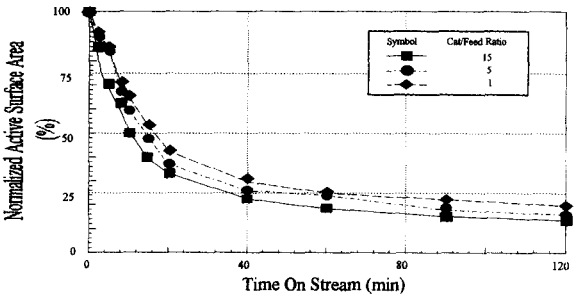

Fig. 6. Experimental results of catalyst/feed ratio effect on surface area loss with time.

reflected from the catalyst surface area against process time plots as shown in Fig. 6, in which more surface area are lost at high W/F.

4.2. Simulated coking from corrugated parallel bundle pore model

The overall coke laydown process simulated from the corrugated parallel bundle pore model is shown in Fig. 7a–d. The catalyst pore elements are free from coke deposits and they are accessible pending on the connectivity in the pore networks (Fig. 7a). As reaction proceeds, coke deposits up to 500 Å thick, which is equivalent to a coke content of 4.5% (Fig. 7b). When the coke layer reaches 1000 Å (6.8% coke content), some totally blocked micropores and a number of partially closed macropores are clearly indicated (Fig. 7c). The coking rate reduces as the coke layer gets thicker, and hence the coke content does not increase very much. The catalyst is fully deactivated when the coke content reaches just over 8% as shown in Fig. 7d from which all the macro and micro pores are totally blocked. Some uncontaminated

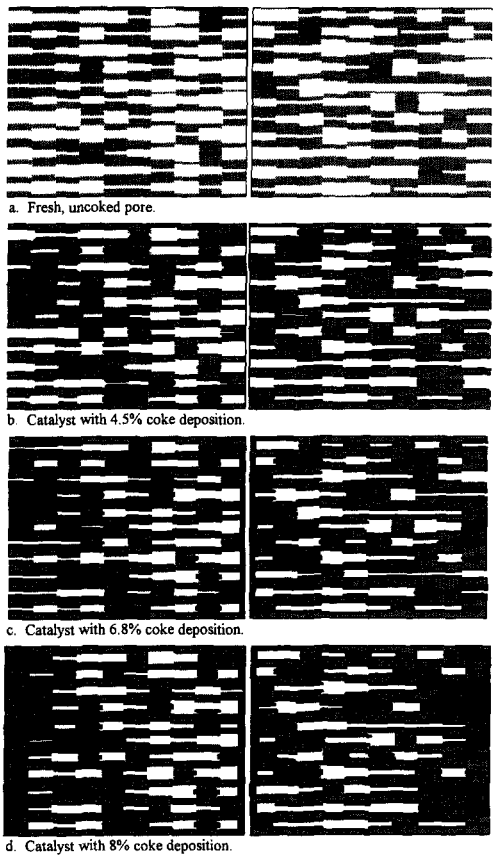

Fig. 7. Different coke levels in the pore under a series coking mechanism. (a) Fresh, uncoked pore, (b) Catalyst with 4.5% coke deposition, (c) Catalyst with 6.8% coke deposition and (d) Catalyst with 8% coke deposition.

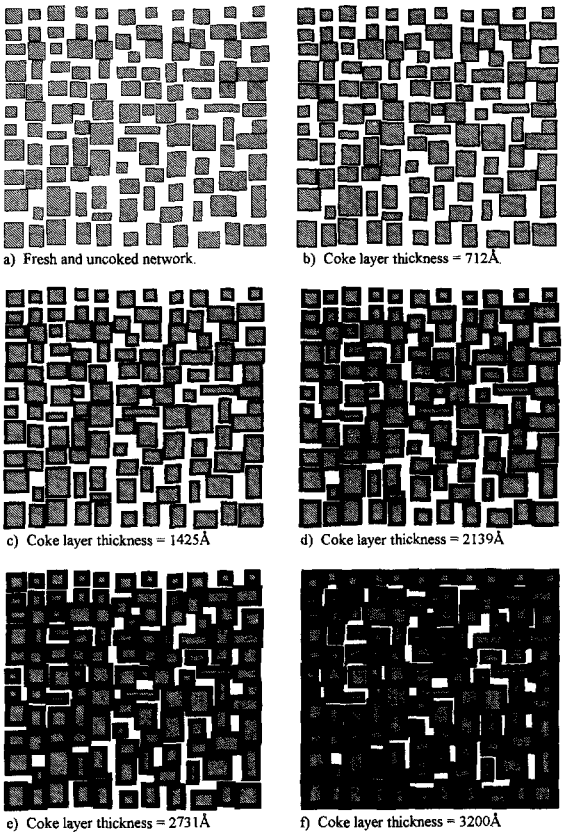

Fig. 8. A schematic 10 × 10 stochastic network with uniform pore size distribution (60–3200 Å). (a) Fresh and uncoked network, (b) Coke layer thickness = 712 Å, (c) Coke layer thickness = 1425 Å, (d) Coke layer thickness = 2139 Å, (e) Coke layer thickness = 2731 Å and (f) Coke layer thickness = 3200 Å.

pore elements still exist, but they are inaccessible. This is similar to the experimental results from the cracking of cumene over the zeolite catalyst and catalyst deactivation by coke laydown as shown in Figs. 4, 5 and 6. Clearly, at high conversion levels, the coking rates indicated by the slopes of the coke content with process time were substantial. In contrast, at low conversions, reversed trends were observed which are the typical characteristics in series fouling [15,16].

4.3. *Simulated coking from the stochastic network pore model*

In this overall coke laydown simulation, the catalyst structure is represented by a 10 × 10 network with a uniform pore size distribution between 60–3200 Å. A fresh catalyst is shown in Fig. 8a. The pore connectivity is excellent and no isolated pore is present. As the reaction proceeds, the coke layer increases from 0 to 712 Å. Fig. 8b shows that the pores with size less than 712 Å are blocked. When the coke layer reaches 1425 Å, the closure of more pore channels is apparent but no isolated pore is formed as illustrated in Fig. 8c. The pore isolation phenomenon emerges when the coke layer reaches 2139 Å which is equivalent to a 12% coke content, see Fig. 8(d). The pore isolation becomes more severe when the coke layer approaches 2731 Å, while some pores are only partially coked, Fig. 8(e). When the catalyst is completely deactivated at the coke thickness of 3200 Å, the coke content is just over 15% in which 6% of the total pore network

Table 2
Comparison of characterization values

Parameters	Measured value	Corrugated parallel bundle model	Stochastic network pore model
Pore length (μ)	—[a]	14	14
Zeolite unit cell (Å)	—[a]	1.0	1.2
Support unit cell (Å)	20.25	20.00	23.00
Pore size distribution (Å)	60–3200	60–3200	60–3200
Zeolite fractional activity	—[a]	0.5	0.86

[a] Analytical method not available.

has been isolated by pore plugging. However, this may change if the pore connectivity, deactivation reaction controlling regime or coking mechanism is modified.

4.4. *Parameter estimation of structured catalyst characterization*

Both the corrugated parallel bundle pore and stochastic network pore models are then applied to simulate the coke content in a fluidized-bed reactor in which the series fouling mechanism is assumed. After undertaking several simulation experiments to determine the best fitted values of coking reaction parameters, the optimized values were obtained and listed in Table 2 for catalyst deactivation. The simulated values of the catalyst support unit cell size and pore size distribution are compared well with those obtained from experimental findings. In addition, a number of catalyst characterization parameters which cannot be measured from the available equipment can be estimated. For example, the pore length is estimated to be 14 μ from both models, zeolite unit cell size of 1.0 and 1.2 Å [17], as well as zeolite fractional activity of 0.5 and 0.86 from the corrugated parallel bundle pore model and stochastic network pore model, respectively. A comparison of the coke content with process time from the experimental data and simulated results from both models is given in Fig. 9. The prediction of coke content as a function of time from the network model compare very well with the observed deactivation behaviour in the commercial catalyst under catalyst deactivation from cracking of cumene in a fluidized bed reactor for all the three values of catalyst to fed ratio of 1, 5 and 15. However, the prediction from the corrugated parallel bundle pore model are generally higher than those of the experiments.

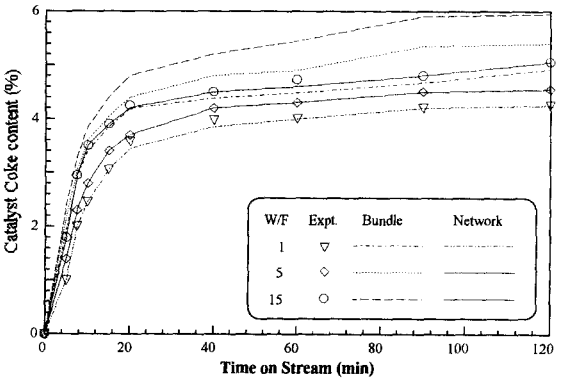

Fig. 9. Comparison of model predictions and experimental data.

5. Conclusions

The theoretical and practical aspects of the deactivation by coking of a commercial supported zeolite catalyst has been investigated. Deactivation studies were carried out in a laboratory scale fluidized bed reactor to disproportionate cumene as the model reaction. To interpret the experimental results, an analysis for cumene conversion, benzene selectivity and coke deposition in catalyst has been developed. The material balance over the reactor system for the cumene can be determined precisely within 4%. The benzene selectivity was found to increase with time on stream. The deactivation due to coking is found to be followed by a series of fouling mechanism.

Theoretical models of 'corrugated parallel pore' and 'stochastic network pore' have been developed to study catalyst coke deposition based on the interaction of the geometries of the coke particles and the pore structures. The graphical illustrations of coke deposition in the pore structures with process time in term of pore structures, pore connectivity, existence of

isolated pore and pore plugging phenomena can be visualized. A number of characterization parameters which cannot be obtained from the existing analytical methods can be estimated from the models, while those measurable ones are compared well with those from the models. The prediction of coke content as a function of time from the stochastic network pore model fitted very well with the observed deactivation behaviour in the commercial catalyst.

6. Notations

A_{OS}	fraction of active area in a pore element
$C_A(x)$	point concentration in a pore element
$C_{A,n}$	concentration between pore elements n and $n-1$
C_F	mean product concentration
D_n	diffusion coefficient in a pore element, m^2/s
d_z	size of coke unit in zeolite microscope, Å
k_{cp}	surface reaction rate constant, m^2/s
L	length of a pore element, m
M,M	mean depth of coke units in a pore element and in zeolite, respectively, Å
M_c, M_b	molecular weights for cumene and benzene, respectively, g/mol
m_n	reaction modulus for pore element n
n, N	nth and total number of elements in a pore, respectively, used in the corrugated parallel bundle model
n	total number of elements in a pore used in the stochastic network pore model
P	total number of pores in a catalyst particle
$P(t_i)$	liquid product mass from normal run at time t, g
$P_b(t_i)$	liquid product mass from 'blank' run at time t_i; g
Q	total flow along a pore
$R(0)$	initial radius of a pore element
$R(t)$	average radius of a pore element at time t
R_n	radius of pore element n
$-r_A$	reaction rate of reactant A
$S(t)$	normalized total benzene selectivity at any time t
$S_d(t_i)$	benzene selectivity at time t_i;
$S_i(t)$	total benzene selectivity at any time t
S_g	specific active surface area of zeolite m^2/kg
S_n	total active surface area in a pore element n
t_i	time on stream between two sampling intervals, min
t	process time, h
$V_c(t)$	specific coke content of the catalyst
V_g	specific support volume
v_m, $V_m(t)$	volume and specific coke content of a zeolite micropore, respectively
v_s, $V_s(t)$	volume and specific coke content of a support pore, respectively
v_z, $V_z(t)$	volume and specific volume of zeolite loss in a pore element, respectively
W/F	catalyst to feed ratio
$X(t)$	total cumene conversion at any time t
$X_b(t_i)$	mass fraction of benzene in liquid at time t_i
$X_c(t_i)$	mass fraction of unconverted cumene at time t_i
$X_d(t_i)$	mass fraction of cumene conversion at time t_i
x	length coordinate of pore element

Acknowledgements

The author likes to thank Dr. R. Mann in Chemical Engineering Department, UMIST, UK; and Ms. K. Al-Dolama and Mr. D. Behzad in the Catalyst Characterization Laboratory, KISR, Kuwait.

References

[1] P.B. Venuto and E.T. Habib, Cat. Rev. Sci. Eng., 18 (1978) 1.
[2] D.E.W. Vaughan, Chem. Soc., 33 (1979) 294.
[3] K. Rajagopalan and E.T. Habib Jr., Hydrocarbon Process., Sept. (1992) 43.
[4] D.L. Cresswell, Appl. Catal., 15 (1985) 103.
[5] C. McGreavy, L. Draper and E.K.T. Kam, Chem. Eng. Sci., 49 (1994) 5413.
[6] D. Nicholson and J.H. Petropoulos, J. Phys. D., 1 (1968) 1379.
[7] G.P. Androutsopoulos and R. Mann, Chem. Eng. Sci., 33 (1978) 673.
[8] W.T. Mo and J. Wei, Chem. Eng. Sci., 41 (1986) 703.
[9] V.N. Burganos and S.V. Sotirchos, Chem. Eng. Sci., 44 (1989) 2629.
[10] M.P. Hollewand, L.F. Gladden and C.N. Kenny, 1991, I. Chem. E. Research. Event, Cambridge, pp. 999.

[11] C. McGreavy, E.K.T. Kam, J.S. Andrade Jr. and K. Rajagopal, 1991, The 1st. Anglo–Japanese Symposium on Catalysis, Tokyo, Japan, pp. 1.
[12] O.H.J. Muhammad, PhD. Thesis, University of Manchester Institute of Science and Technology, Manchester, 1992.
[13] G. Thomson, PhD. Thesis, University of Manchester, Manchester, 1986.
[14] O.H.J. Muhammad, Stud. Surf. Sci. Catal., 100 (1996) 365.
[15] M. Viner and B. Wojciechowski, Can. J. Chem. Eng., 62 (1984) 870.
[16] F. Mandani, E.K.T. Kam and R. Hughes, Stud. Surf. Sci. Catal., 100 (1996) 427.
[17] R. Mann, P. Starrat and G. Thomson, Chem. Eng. Sci., 41 (1986) 708.